Molecular Systems Biology (2005) doi:10.1038/msb4100032

www.molecularsystemsbiology.com
Article number: 2005.0024

molecular systems biology

REPORT

Monitoring dynamics of single-cell gene expression over multiple cell cycles

Scott Cookson[1,3], Natalie Ostroff[1,3], Wyming Lee Pang[1,3], Dmitri Volfson[1,2] and Jeff Hasty[1,*]

[1] Department of Bioengineering, University of California at San Diego, La Jolla, CA, USA and [2] Institute for Nonlinear Science, University of California at San Diego, La Jolla, CA, USA
[3] These authors contributed equally to this work
* Corresponding author. Department of Bioengineering, University of California at San Diego, 9500 Gilman Drive, La Jolla, CA 92093-0412, USA.
Tel.: +1 858 822 3442; Fax: +1 309 273 0130; E-mail: hasty@ucsd.edu

Received 11.7.05; accepted 27.10.05

Recent progress in reconstructing gene regulatory networks has established a framework for a quantitative description of the dynamics of many important cellular processes. Such a description will require novel experimental techniques that enable the generation of time-series data for the governing regulatory proteins in a large number of individual living cells. Here, we utilize microfabrication to construct a Tesla microchemostat that permits single-cell fluorescence imaging of gene expression over many cellular generations. The device is used to capture and constrain asymmetrically dividing or motile cells within a trapping region and to deliver nutrients and regulate the cellular population within this region. We illustrate the operation of the microchemostat with *Saccharomyces cerevisiae* and explore the evolution of single-cell gene expression and cycle time as a function of generation. Our findings highlight the importance of novel assays for quantifying the dynamics of gene expression and cellular growth, and establish a methodology for exploring the effects of gene expression on long-term processes such as cellular aging.
Molecular Systems Biology 22 November 2005; doi:10.1038/msb4100032
Subject Categories: functional genomics; synthetic biology
Keywords: gene regulation; microfluidics; microscopy

Introduction

Systems biology has grown rapidly in the wake of the human genome project, as it has become clear that an integration of experimental and computational research will be required to quantitatively describe complex biological systems. The utilization of high-throughput technologies has led to the successful reconstruction of gene regulatory networks in many organisms (Tavazoie *et al*, 1999; Ideker *et al*, 2001; Ibarra *et al*, 2002; Gardner *et al*, 2003), along with the development of quantitative models for many complex and fundamental cellular processes (Vogelstein *et al*, 2000; Simon *et al*, 2001; Breeden, 2003; Bartek *et al*, 2004; Begley and Samson, 2004; Kohn and Pommier, 2005). To complement the progress of genome-scale measurement technologies, a primary focus of synthetic biology is to model and construct novel genetic circuits that reproduce the behavior of natural systems and contribute to our understanding of how complex biological functions arise from the connectivity of gene regulatory networks (Hasty *et al*, 2002; Mangan *et al*, 2003; Basu *et al*, 2005; Pedraza and v Oudenaarden, 2005; Rosenfeld *et al*, 2005). The significant potential of synthetic biology will rest on the development of new tools both for the acquisition and processing of data from large samples of individual cells (Thompson *et al*, 2004; Tourovskaia *et al*, 2005), which will facilitate the characterization of both native and synthetic biological systems. The utility of single-cell measurements with high temporal resolution has been demonstrated by recent bacterial studies, which used optical microscopy to observe *Escherichia coli* over long time periods and reveal interesting temporal fluctuations and cell–cell variability that would otherwise be masked by population-wide measurements (Pedraza and v Oudenaarden, 2005; Rosenfeld *et al*, 2005). However, traditional microscopy methods, which typically involve viewing cells on a microscope slide or an agar plate, limit both the length and quality of an experimental run, as large groups of cells tend to grow out of the focal plane.

Microfabrication (Duffy *et al*, 1999; Hansen and Quake, 2003) can be used to construct custom microfluidic devices in which cells can be cultured in a tightly regulated microenvironment (Balagaddé *et al*, 2005; Groisman *et al*, 2005). Here, we present the development and application of a 'free-running' microfluidic platform tailored to the generation and analysis of single-cell fluorescence data over many cellular generations. We demonstrate the utility of the platform with experimental data acquired from *Saccharomyces cerevisiae*, a workhorse for eukaryotic cell biology. In addition, we present software designed for the extraction of time-series data from a sequence

of fluorescence images. The availability of this device should greatly aid quantitative modelers of both native and synthetic genetic circuits by facilitating the long-term observance of dynamical properties of gene regulation in *S. cerevisiae* and other model organisms.

Results and discussion

The Tesla microchemostat (TμC) is based on an implementation of the classic Tesla diode loop (Tesla 1920; Duffy *et al*, 1999; Bendib and Français, 2001), modified for the imaging of a monolayer culture of cells growing in exponential phase for many generations. The construction is such that the side-arm of the diode forms a shallow trapping region that constrains a population of cells to the same focal plane (Figure 1). Fluid flow is utilized to continuously purge cells that grow beyond the trapping region boundaries so that the device can function as a standard chemostat. Coupled with optical autofocus, this design feature allows for the TμC to operate in 'free-run' mode over long time periods without the need for external adjustment.

In order to achieve free-running long experimental runs, a critical design objective was to avoid clogging between the media port and the trapping region. We developed a three-port chip design in which the main channel extending from the cell port splits into both a media channel and a waste channel downstream of the trapping region, which prohibits the collection of cells in the media port during the loading process (Figure 1A). By constructing the height of the bypass channel to be two or three times the height of the trapping region, substantial flow can be maintained throughout this channel while flow through the trapping region remains minimal. Once cells are loaded, they receive nutrients via a combination of diffusion and advection. As the colony grows, fluidic resistance increases through the trapping region, and diffusion dominates the transport process (see Supplementary information for a detailed analysis of nutrient transport). Supplied with abundant nutrients, the cells are able to grow exponentially to fill the trapping region in a monolayer (Figures 1C and D). The open walls of the trapping region allow for peripheral cells to escape when they are pushed into the high flow of the main channel, thus permitting continuous exponential growth long after the trapping region becomes full.

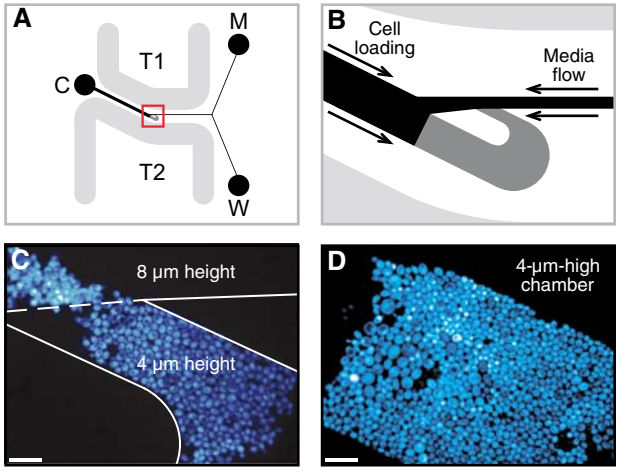

Figure 1 The TμC design was optimized to allow for long-term growth of cells in a monolayer. (**A**) Three separate ports for cell loading (C), media supply (M), and waste (W) minimize potential clogging of media supply lines. With this layout, we are able to generate optimal fluid flow both for the loading of cells into the trapping region and for the delivery of nutrients over many generations. Strong flow toward the trapping region provides the momentum necessary to carry cells into the region against high resistance. Cells that do not enter the trapping region are forced into the waste port by strong flow from the media port. Once cells are loaded, flow is reversed to run from the media port to both the waste and cell ports. Running temperature-regulated water through thermal lines T1 and T2 maintains the device at an optimal temperature. (**B**) A zoomed-in view of the diode loop. The height of the trapping region (dark gray) is customized based on species. The flow channels (black) are 2–3 times higher than the trapping region. An open trapping region (black/gray interface) allows for peripheral cells to be pushed from the observation region as the colony grows. (**C**) Shallow trapping regions confine cells to a monolayer. Cells residing at the trapping region entrance highlight the benefit of a height-constrained growth environment. Scale bar, 20 μm. (**D**) The 4-μm-high yeast TμC full of cells after 24 h of growth. Scale bar, 20 μm.

Based on these design considerations, the TμC is constructed using well-documented microfabrication techniques (see Materials and methods). Briefly, a poly(dimethylsiloxane) (PDMS) chip is created with the desired channels and microstructures from a patterned silicon wafer template. Device fabrication is relatively straightforward, as it requires only a single PDMS layer. Furthermore, flow control is maintained by passive gravitational forces alone, eliminating the need for complex on-chip actuators, flow circuitry, and run-time software. The minimal three-port design allows for a rapid experimental setup that has been optimized for convenience and requires approximately 1 h of bench time. The simplicity of device construction and experimental setup makes the platform accessible to experimentalists with minimal experience in microfabrication.

We illustrate the utility of the device using the budding yeast *S. cerevisiae,* an excellent test for the TμC device owing to the tendency of cells to flocculate, or aggregate into clumps. This property presents a major obstacle in the attainment of long-term single-cell temporal data in this important model organism (Hartwell *et al*, 1997; Simon *et al*, 2001; Simon and Yen, 2003; Chen *et al*, 2004; McMurray and Gottschling, 2004; Scheibel *et al*, 2004). To address this problem, we designed the trapping region height to be approximately equal to the diameter of a single yeast cell. The significant advantage of monolayer growth in a height-constrained chamber is demonstrated by visualizing the group of cells residing at the trapping region boundary (Figure 1C). The cells growing inside the 4-μm-high cell chamber are collectively in focus, and individual cells can easily be distinguished. In contrast, cells just outside of the chamber, where the height is 8 μm, grow in multiple layers, producing blurry aggregates from which quantitative single-cell data are very difficult to extract using wide-field microscopy. Although this may not impede the observation of a few cells over a short period of time, as these cells begin to divide it becomes increasingly difficult to resolve individual cells and quantify their behavior.

Using the TμC device to grow a monolayer colony of cells, we can obtain a long sequence of consistently focused fluorescence images (see Supplementary Movie 1). The extraction of single-cell expression dynamics from a sequence of images involves two major steps: (i) we segment each image into individual cells and (ii) we resolve the temporal evolution from the segmented images (see Supplementary information

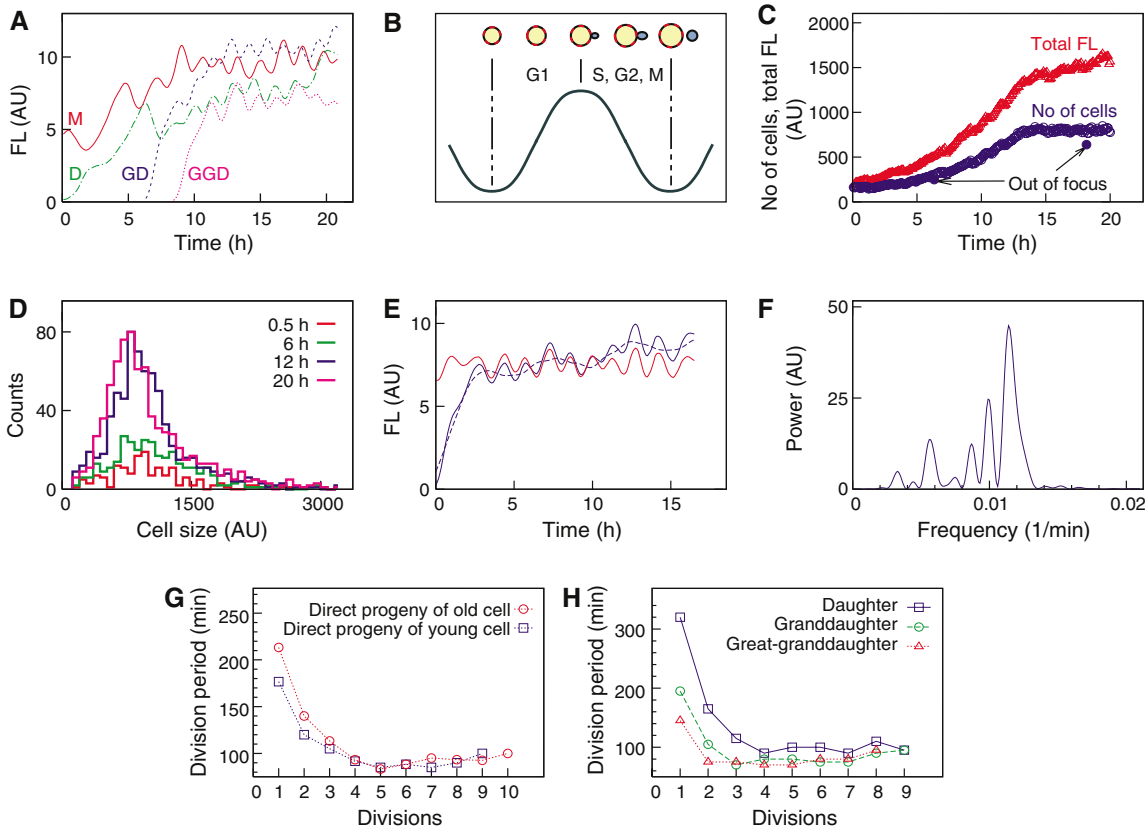

Figure 2 (**A**) Four representative, directly related (mother, daughter, granddaughter, great-granddaughter) trajectories showing fluorescence of each cell as a function of time. (**B**) Cartoon illustrating how the cell tracking leads to oscillations in a gene expression time series. (**C**) Total number of segmented cells as a function of time and the sum of the fluorescent signals of all cells as a function of time. (**D**) Histograms of cell sizes at various times throughout the experiment. (**E**) Data processing: raw data smoothed with an 8-point Savitsky–Golay filter (solid blue line); long-term trend obtained with a 45-point Savitsky–Golay filter (dashed blue); detrended data input to Lomb–Scargle transform (solid red). (**F**) Sample frequency spectrum of a typical trajectory, where the 0.0116 1/min frequency peak corresponds to a cell division period of 86.1 min. (**G**) The time per division versus division number for progeny of a nearly senescent cell and progeny of a younger cell. Each curve is averaged over three cells. (**H**) The time per division versus division number for the daughter, granddaughter, and great-granddaughter of a nearly senescent cell.

and Supplementary Movie 3). We utilized cells that exhibit galactose-dependent expression of yeast-enhanced Venus fluorescent protein (yEVFP) from three integrated copies of the *GAL1* promoter driving yEVFP. Fully induced cells are tracked through a series of images, yielding fluorescence trajectories that rise and fall with each cell cycle (Figures 2A and 3). Since segmentation involves tracking a daughter cell from the moment the bud begins to emerge, the fluorescence signal of the mother is observed to decrease as yEVFP freely diffuses to the bud throughout the S, G2, and M phases. The fluorescence signal rises again at the beginning of the next G1 phase, when the mother and daughter have fully divided and the mother can resume the accumulation of fluorescent protein (Figure 2B). The cell count grows exponentially until the chamber fills, at which point the chemostat enables extended run-times as the population can continue growing by pushing peripheral cells out of the trapping region (Figure 2C). Histograms of cell sizes at different time points throughout the experiment retain a constant distribution, indicating that growth conditions remain optimal for the duration of the run (Figure 2D).

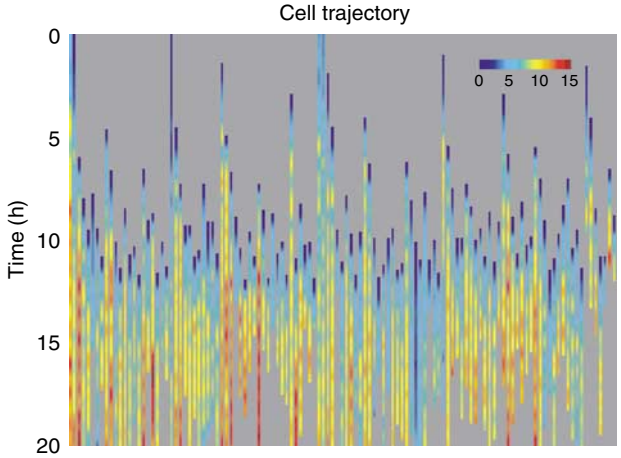

Figure 3 Single-cell yellow fluorescent protein (YFP) dynamics for 119 cells. Each column corresponds to a density plot that depicts the evolution of the amount of YFP in a single cell over a period of many hours (the scale bar denotes arbitrary units consistent with Figure 2). Variations in cycle times and long-term trends are clearly discerned. The dynamics of YFP production and division were generated from the cells shown in Supplementary Movie 1.

The most novel utility of the TμC is the ability to observe single-cell dynamics over long time periods. Quantitative accuracy of the fluorescence trajectories can be ensured by compensating for errors that may be introduced by experimental conditions and image analysis (see Supplementary information). These trajectories can be used to extract many types of information about individual cells, such as the average cell cycle time for any individual cell (Figures 2E and F). We can also use fluorescence to monitor how the division rate of an individual cell evolves as it ages. Given that the local minima of a trajectory mark the beginning of each G1 phase, we can calculate the duration of each cell division as the time between each G1 start. As expected, the first cell cycle of a new bud is unusually long, as the bud first has to grow to a certain size before it can begin producing buds of its own. However, our fluorescence data suggest that it often takes a young cell two or three cycles to recover to a normal division rate (Figure 2G). This phenomenon is particularly pronounced in daughters of old, nearly senescent cells, as reported in various studies of aging in yeast (Egilmez and Jazwinski, 1989). Figure 2G compares the evolution of division times for direct progeny of an old cell and direct progeny of a young cell, averaged over three examples of each. For progeny of the young cell, we see that the first division time is long, as expected, and then the cells quickly recover down to a steady division rate. In contrast, progeny of older cells take longer to reach this steady state, as indicated by the longer division times for the first few cell cycles. This phenomenon is highlighted in Figure 2H, where the division times for the daughter, granddaughter, and great-granddaughter of a nearly senescent cell are plotted. We observe that the daughter takes three cycles to recover to steady state, the granddaughter takes two cycles to recover, and the great-granddaughter recovers immediately. These cycle-time results are consistent with previous studies that utilized different assays (Egilmez and Jazwinski, 1989), and the ability to simultaneously track gene expression over long periods highlights the utility of the device.

The ability to perform long-duration experiments that yield consistent single-cell data is critical for the generation of computational models with predictive abilities, a hallmark of synthetic biology. We have demonstrated the utility of a novel microchemostat that can be used for monitoring cellular dynamics over many generations. This device offers a number of significant technical advantages over existing methods such as flow cytometry and traditional microscopy. Flow cytometry provides a snapshot of single-cell data, but does not offer the ability to dynamically track a given single cell. These population measurements provide very useful information about the steady-state behavior of biological networks, but they inherently sacrifice details at the single-cell dynamical level. Traditional microscopy assays yield useful and very detailed information on the dynamical behavior of a small number of cells but typically run only for a short time period and sacrifice the ability to generate good statistics over a population. In contrast, the TμC we have designed and developed allows for long-term single-cell dynamical measurements over a large population. Within the context of systems biology, the ability to generate such data at the single-cell level will aid in the development of predictive dynamical modeling (Chen *et al*, 2004) and facilitate the application of novel approaches such as the use of frequency-space analysis to quantify the variability inherent in gene expression (Simpson *et al*, 2003). The unique capability of the TμC for studying both the dynamics and the variability of biological processes within a population of living cells represents an important step toward bringing quantitative single-cell data to the field of systems biology.

Materials and methods

Fabrication procedure

Microfluidic devices were constructed using well-established techniques (Duffy *et al*, 1999; Hansen and Quake, 2003) and the UCSD Integrated Technology Lab (ITL). Briefly, photolithographic photomasks were drawn using FreeHand MX (Macromedia Inc., San Francisco, CA), printed onto transparency film at high resolution (Output City, Poway, CA), and mounted to clean borosilicate glass plates (McMaster-Carr, Los Angeles, CA). To make master molds, SU-8 2000 (MicroChem Corp., Newton, MA) was spin coated to appropriate depths using a Headway PWM32 programmable spinner (Headway Research Inc., Garland, TX) and patterned by UV exposure via appropriate photomasks using a contact mask aligner (HTG, San Jose, CA). After all photolithographic steps were completed, SU-8 feature heights were verified using a DEKTAK 3030ST profilometer (Sloan Technology Corp., Santa Barbara, CA), and treated with vaporous chlorotrimethylsilane for 5–10 min. PDMS/Sylgard 184 (Dow Corning, Midland, MI) was mixed in a 10:1 ratio with the supplied crosslinking agent and degassed in a vacuum desiccator at −15 mmHg for 30 min to 1 h. The degassed PDMS was then poured over the silicon/SU-8 master to a depth of approximately 0.5 cm and cured at 80°C for 1 h. After curing, the hardened PDMS monolith was carefully released from the master. Fluidic ports for media/cell loading and heated water lines were bored with 20- and 16-gauge Luer stub adapters, respectively, and flushed with 0.2-μm-filtered dH_2O. Individual chips were sectioned from the PDMS monolith and sonicated in a 0.1% v/v Tween 80 solution for 15 min and rinsed in dH_2O. Scotch 810 office tape was used to remove any remaining particles from the PDMS surface. Finally, each chip was exposed to O_2 plasma for 30 s in a Technics 500-II Plasma Asher and brought into contact with plasma-cleaned 24×40 mm No $1\frac{1}{2}$ coverslips (Corning Inc., Corning, NY), which forms a strong irreversible bond between the two surfaces (Wu *et al*, 2002). Our photomask files are freely available for academic use and may be downloaded from our website (http://biodynamics.ucsd.edu/download.html).

Loading procedure

In preparation for cell observation, devices were mounted to the microscope stage and connected to thermal water baths to maintain the optimal growth temperature of 30°C. Thermal connections were made using Tygon microbore tubing (0.050 in ID, 0.090 in OD) (Cole Parmer, Vernon Hills, IL) connected to chip thermal ports with 16-gauge dispensing needles (McMaster-Carr, Los Angeles, CA). Water temperatures flowing into and out of the device were monitored using in-line thermocouples. Following device priming with filtered dH_2O, an open 10 ml syringe serving as a waste reservoir was filled with media and suspended 5 in above the device. A similar media connection was made at the device media port at a height of 25 in. Cells and 2.5-μm-diameter YG fluorescent beads were loaded into the device at the cell port, with the beads serving as a fluorescence intensity standard, until several of each entered the trapping region. During loading, all flows were directed toward the waste port to prevent contamination of the media line. To minimize clogging, strong flow from the media port was used to flush clear all cells residing in the shared fluid channels. Finally, the three reservoirs were brought to their final run-time heights, with the cell reservoir fixed at a height 1 in above the waste reservoir and the media reservoir fixed at a height 1 in above the cell reservoir. These differential heights provided for

both gentle flow of media through the trapping region and strong flow of media into the waste port, thereby feeding the cells to be monitored while preventing discarded cells from re-entering the system.

Strain and cell culture

The yeast strain was created by targeted chromosomal integration of the pRS61-yv vector at the Gal1-10 locus of *S. cerevisiae* strain K699 (a, ADE2, ura3, his3, trp1, leu2). The vector was constructed using standard recombination techniques from two commercially available vectors: the tryptophan marker from pRS404 was inserted into the pESC-His vector, which contains the Gal1-10 promoter locus of *S. cerevisiae* (see Supplementary Figure S8). yEVFP, a yellow fluorescent protein (YFP) variant, was inserted behind the Gal1 promoter for fluorescence production inducible by the addition of galactose to the medium. Cultures were grown in synthetic drop-out (SD) medium supplemented with all amino acids except histidine for selection of the correct integrant and containing 2% glucose. After selection, cultures were grown in SD supplemented with all amino acids and containing 2% galactose for full induction of the production of the yEVFP. To minimize flocculation of yeast while growing in the incubator shaker, single colonies were initially inoculated into 1 ml of medium in a microcentrifuge tube and vortexed on high for 2 min before being transferred to a culture tube with 4 ml total medium. Cultures were then grown at 30°C for 18–24 h to an OD_{600} of 1.0 ± 0.25. In preparation for loading, four samples from a single culture were diluted into 1 ml of medium in a microcentrifuge tube to an OD_{600} of 0.05 and vortexed for 5–10 min. Cultures were then combined with 4 ml of total culture for loading into the chip.

Data acquisition

Image acquisition was performed on a Nikon Diaphot TMD epifluorescent inverted microscope outfitted with fluorescence excitation and emission filter wheels, an XY motorized stage and fine focus motor with a hardware-based autofocus controller (Prior Scientific, Rockland, MA), and Uniblitz VS35 high-speed shutters (Vincent Associates, Rochester, NY) mounted in the fluorescence and transmitted light paths. Images were acquired using a Hamamatsu ORCA-ERG cooled CCD camera and a custom positioning and multispectral acquisition application written in LabVIEW (National Instruments, Austin, TX). Imaging for the autofocus controller was performed using a COHU 4900 series CCTV camera mounted to one of the microscope eyepieces. Fluorescence visualization was performed with narrow band-pass excitation and emission filters for RFP and YFP (Chroma Inc., Rockingham, VT) for beads and yEVFP, respectively.

Supplementary information

Supplementary information is available at the *Molecular Systems Biology* website (www.nature.com/msb).

Acknowledgements

We thank Dmitri Bratsun for design suggestions based on the Tesla diode, Ting Lu for assistance in analyzing the flow properties of the diode, and Alex Groisman for technical advice on microfabrication. This work was supported by the NSF Division of Cellular and Molecular Bioscience, the Alfred P Sloan Foundation (JH), the DOE CSGF (NO), and the DOD NDSEG Fellowship Program (SC).

References

Balagaddé FK, You L, Hansen CL, Arnold FH, Quake SR (2005) Long-term monitoring of bacteria undergoing programmed population control in a microchemostat. *Science* **309:** 137–140

BarteK J, Lukas C, Lukas J (2004) Checking on DNA damage in S phase. *Nat Rev Mol Cell Biol* **5:** 792–804

Basu S, Gerchman Y, Collins CH, Arnold FH, Weiss R (2005) A synthetic multicellular system for programmed pattern formation. *Nature* **434:** 1130–1134

Begley TJ, Samson LD (2004) Network responses to DNA damaging agents. *DNA Repair (Amst)* **3:** 1123–1132

Bendib S, Français O (2001) Analytical study of microchannel and passive microvalve 'application to micropump simulator'. In *Design, Characterisation, and Packaging for MEMS and Microelectronics 2001*, Adelaide, Australia, pp 283–291

Breeden LL (2003) Periodic transcription: a cycle within a cycle. *Curr Biol* **13:** R31–R38

Chen KC, Calzone L, Csikasz-Nagy A, Cross FR, Novak B, Tyson JJ (2004) Integrative analysis of cell cycle control in budding yeast. *Mol Biol Cell* **15:** 3841–3862

Duffy DC, Schueller OJA, Brittain ST, Whitesides GM (1999) Rapid prototyping of microfluidic switches in poly(dimethyl siloxane) and their actuation by electro-osmotic flow. *J Micromech Microeng* **9:** 211–217

Egilmez NK, Jazwinski SM (1989) Evidence for the involvement of a cytoplasmic factor in the aging of the yeast *Saccharomyces cerevisiae*. *J Bacteriol* **171:** 37–42

Gardner TS, D Bernardo D, Lorenz D, Collins JJ (2003) Inferring genetic networks and identifying compound mode of action via expression profiling. *Science* **301:** 102–105

Groisman A, Lobo C, Cho H, Campbell JK, Dufour YS, Stevens AM, Levchenko A (2005) A microfluidic chemostat for experiments with bacterial and yeast cells. *Nat Methods* **2:** 685–689

Hansen C, Quake SR (2003) Microfluidics in structural biology: smaller, faster …better. *Curr Opin Struct Biol* **13:** 538–544

Hartwell LH, Szankasi P, Roberts CJ, Murray AW, Friend SH (1997) Integrating genetic approaches into the discovery of anticancer drugs. *Science* **278:** 1064–1068

Hasty J, McMillen D, Collins JJ (2002) Engineered gene circuits. *Nature* **420:** 224–230

Ibarra RU, Edwards JS, Palsson BO (2002) *Escherichia coli* K-12 undergoes adaptive evolution to achieve *in silico* predicted optimal growth. *Nature* **420:** 186–189

Ideker T, Thorsson V, Ranish JA, Christmas R, Buhler J, Eng JK, Bumgarner R, Goodlett DR, Aebersold R, Hood L (2001) Integrated genomic and proteomic analyses of a systematically perturbed metabolic network. *Science* **292:** 929–934

Kohn KW, Pommier Y (2005) Molecular interaction map of the p53 and Mdm2 logic elements, which control the Off–On switch of p53 in response to DNA damage. *Biochem Biophys Res Commun* **331:** 816–827

Mangan S, Zaslaver A, Alon U (2003) The coherent feedforward loop serves as a sign-sensitive delay element in transcription networks. *J Mol Biol* **334:** 197–204

Mcmurray MA, Gottschling DE (2004) Aging and genetic instability in yeast. *Curr Opin Microbiol* **7:** 673–679

Pedraza JM, v Oudenaarden A (2005) Noise propagation in gene networks. *Science* **307:** 1965–1969

Rosenfeld N, Young JW, Alon U, Swain PS, Elowitz MB (2005) Gene regulation at the single-cell level. *Science* **307:** 1962–1965

Scheibel T, Bloom J, Lindquist SL (2004) The elongation of yeast prion fibers involves separable steps of association and conversion. *Proc Natl Acad Sci USA* **101:** 2287–2292

Simon I, Barnett J, Hannett N, Harbison CT, Rinaldi NJ, Volkert TL, Wyrick JJ, Zeitlinger J, Gifford DK, Jaakkola TS, Young RA (2001) Serial regulation of transcriptional regulators in the yeast cell cycle. *Cell* **106:** 697–708

Simon JA, Yen TJ (2003) Novel approaches to screen for anticancer drugs using *Saccharomyces cerevisiae*. *Methods Mol Biol* **223:** 555–576

Simpson ML, Cox CD, Sayler GS (2003) Frequency domain analysis of noise in autoregulated gene circuits. *Proc Natl Acad Sci USA* **100:** 4551–4556

Tavazoie S, Hughes JD, Campbell MJ, Cho RJ, Church GM (1999) Systematic determination of genetic network architecture. *Nat Genet* **22:** 281–285

Tesla N (1920) US patent no. 1,329,559, 03 February 1920

Thompson DM, King KR, Wieder KJ, Toner M, Yarmush ML, Ja-Yaraman A (2004) Dynamic gene expression profiling using a microfabricated living cell array. *Anal Chem* **76:** 4098–4103

Tourovskaia A, Figueroa-Masot X, Folch A (2005) Differentiation-on-a-chip: a microfluidic platform for long-term cell culture studies. *Lab Chip* **5:** 14–19

Vogelstein B, Lane D, Levine AJ (2000) Surfing the p53 network. *Nature* **408:** 307–310

Wu ZY, Xanthopoulos N, Reymond F, Rossier JS, Girault HH (2002) Polymer microchips bonded by O_2-plasma activation. *Electrophoresis* **23:** 782–790